A Novel Method for Structure-Based Prediction of Ion Channel Conductance Properties

Oliver S. Smart,* Jason Breed,# Graham R. Smith,# and Mark S. P. Sansom#
*Department of Crystallography, Birkbeck College, The University of London, London WC1E 7HX, and #Laboratory of Molecular Biophysics, The Rex Richards Building, University of Oxford, Oxford OX1 3QU, England

ABSTRACT A rapid and easy-to-use method of predicting the conductance of an ion channel from its three-dimensional structure is presented. The method combines the pore dimensions of the channel as measured in the HOLE program with an Ohmic model of conductance. An empirically based correction factor is then applied. The method yielded good results for six experimental channel structures (none of which were included in the training set) with predictions accurate to within an average factor of 1.62 to the true values. The predictive r^2 was equal to 0.90, which is indicative of a good predictive ability. The procedure is used to validate model structures of alamethicin and phospholamban. Two genuine predictions for the conductance of channels with known structure but without reported conductances are given. A modification of the procedure that calculates the expected results for the effect of the addition of nonelectrolyte polymers on conductance is set out. Results for a cholera toxin B-subunit crystal structure agree well with the measured values. The difficulty in interpreting such studies is discussed, with the conclusion that measurements on channels of known structure are required.

1. INTRODUCTION

Over the past 40 years structural studies on globular proteins have produced a revolution in the understanding of the fundamental basis of many biological processes. The application of x-ray and NMR techniques to proteins is now increasingly forming a standard part of biochemical and pharmaceutical studies (Perutz, 1992). Indeed, the number of new globular protein structures being deposited in the Brookhaven Protein Databank (Bernstein et al., 1977; Abola et al., 1987) is approaching three a day. This is in stark contrast to the situation for integral membrane proteins. Difficulty in application of structure determination methods have restricted the amount of information for these systems. However, recently structures have been reported at an increasing rate—in 1990 there was only one experimental structure of an integral membrane protein with a resolution sufficient to produce an atomistic model (Henderson et al., 1990), but at present there are at least 12. Given further methodological development, particularly of NMR (Bloom, 1995) and electron microscopy, we can expect a further revolution in this area.

One of the most important classes of membrane proteins are ion channels. Ion channel activity is crucial to the electrical properties of excitable cells and thus to the action of a large number of neuroactive drugs. In addition, many toxins and antibiotics also act by forming ion channels. Given the importance of these systems and the relative absence of detailed experimental structures, many workers have used modeling and simulation techniques to obtain potential atomic models of channels. These structures are based at best on low-resolution structural information (e.g., electron microscopy data; Unwin, 1993, 1995; Sansom et al., 1995) and more often on a mixture of mutagenesis data and intuition (e.g., Adams et al., 1995).

In a series of detailed studies of the linear gramicidin ($\rightarrow \leftarrow \beta^{6.3}$) channel, for which detailed structural information is available, Roux and Karplus (1991a,b, 1993; Roux, 1995) have developed a methodology that enables the ab initio calculation of the conductance of an ion channel structure. This involves performing extensive molecular dynamics simulations, using the free energy perturbation method (Roux and Karplus, 1993) to calculate a potential of mean force (free energy profile) for the ion passing along the channel. This is then combined with activated molecular dynamics to calculate a reaction rate and a maximum conductance for the channel. Although the method leads to a detailed understanding of the exact processes involved in conduction, the procedure is computationally expensive. All of the problems inherent in any simulation study are entailed, for instance, in finding an adequate representation of the environment (particularly acute in the case of membrane proteins) and developing realistic and consistent potential energy functions.

At present it would be infeasible to predict macroscopic observables such as conductance for many model structures using the methodology set out by Roux and Karplus (1991a,b, 1993; Roux, 1995). A particular difficulty is to discriminate between different structural models of a given conductance state, for instance, to identify the number of helices involved in a helical bundle. To achieve this a comparative analysis must be made between two or more

Received for publication 12 August 1996 and in final form 17 December 1996.

Address reprint requests to Dr. Oliver Smart, Department of Crystallography, Birkbeck College, The University of London, Malet Street, London WC1E 7HX, England. Tel.: +44-171-631-6810; Fax: +44-171-631-6803; E-mail: o.smart@mail.cryst.bbk.ac.uk; www: http://www.cryst.bbk.ac.uk/~ubcg8ab/smart.html.

Dr. Breed's present address is Fakultät für Biologie, Universität Konstanz, Postfach 5560, M656, 78434 Konstanz, Germany.

0006-3495/97/03/1109/18 $2.00

models, thus compounding the computational cost. These problems are most acute for large systems. This leads us to identify the need for an easy-to-use and rapid, yet reasonably accurate method for assigning a conductance to a particular ion channel model.

The method set out in section 2 was developed to rapidly predict the conductance for any given channel model. The aim was to achieve predictions that are reliable to within a factor of 2, a reasonable range given the typical variation in published experimental conductances of a given channel. A modification of the procedure that aims to predict the effect of nonelectrolytes on the conductance properties of a channel is described in section 3. This represents the first attempt to link such experiments (which can be interpreted in terms of structural dimensions of the channel) with detailed atomic structural models. It is shown that given further experimental and computational work, such experiments have the potential to be a powerful aid to modeling studies.

2. PREDICTING THE CONDUCTANCE OF ION CHANNEL ATOMIC MODELS

2.1 Theory

In the standard reference work on ion channels, Hille (1992) sets out a simple but instructive analysis of the conductance of the simplest abstraction of a channel. The model considers a channel as a cylindrical opening of radius R through an impermeable lipid layer of width L. The conductance G is given by

$$G^{-1} = \frac{\rho_{bulk} L}{\pi R^2} + \frac{\rho_{bulk}}{4R} + \frac{\rho_{bulk}}{4R}, \quad (1)$$

where ρ_{bulk} is the resistivity of the permeant ionic solution. The first term is the standard expression for the resistance of a body of length L and uniform cross-sectional area πR^2. The latter two terms represent the access resistance at the two mouths of the pore (Hall, 1975). This is the contribution made to the resistance by the fact that ions must diffuse up to the mouth of the channel, with the conductive media outside the channel. Except for very short, wide channels, the contribution of the access resistance to the total is likely to be below 10% of the total (Hille, 1992). As the method only aims to find an approximate conductance, this term is normally neglected (although it is crucial in analyzing the effect of nonelectrolytes on conductance; see section 3).

Instead of considering a cylindrical conductor, the HOLE program (Smart et al., 1993; Smart, 1996) is used to define an irregularly shaped pore determined by the 3D atomic structure of the channel. The HOLE method uses Monte Carlo simulated annealing to maximize the radius of a sphere that is forced to squeeze through the van der Waals surface of the channel. The user defines a channel direction vector, which is used to define a stack of planes with a uniform separation s. A separate optimization is conducted for each plane, keeping the sphere center on the plane. The restriction to spherical geometry, although reasonable for thin pores, becomes problematic for large channels, which are often clearly anisotropic. For this reason an adaptation (the "capsule" option) was used in which, instead of optimizing a single sphere, a spherocylinder (which can be described in terms of two independently moving centers) is used (Fig. 1 *A*). This feature, which will be more fully described in a separate publication (Smart et al., manuscript in preparation), allows the measurement of anisotropy (Fig. 1 *B*) for a small increase in computational cost (typical runs take a few tens of minutes on a modern workstation). The procedure can be considered to define a series of slabs, normal to the channel vector, of uniform thickness s and area A (whose variation is determined as a function of displacement along the channel vector z).

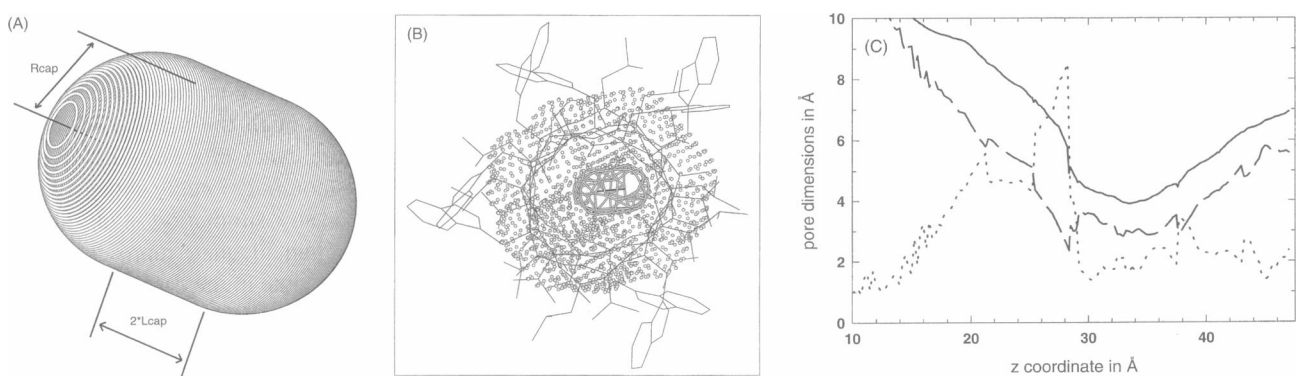

FIGURE 1 The capsule option of the HOLE program uses a spherocylinder to measure the anisotropy of a channel. A spherocylinder (*A*) can be thought of as a sphere whose center has been extended into a line. (*B*) How HOLE optimizes a spherocylinder within the pore of the NMR structure of gramicidin A (Ketchem et al., 1993). The view is down the channel direction vector (i.e., normal to the membrane). A single spherocylinder is shown in a spaghetti representation fitting within a dot surface of surrounding atoms. Note that the long axis of the spherocylinder is always maintained at right angles to the channel direction vector. HOLE optimizes the effective radius of the spherocylinder, which is defined as $(R_{cap}^2 + L_{cap}R_{cap}/\pi)^{1/2}$, i.e., the radius of a circle with the same area as capsule normal to the channel vector. (*C*) The procedure in application to the x-ray crystal structure OmpF porin from *E. coli* (Cowan et al., 1992). The dashed line shows the capsule radius along the channel, the dotted line the capsule length, and the solid line the effective radius. The pore dimensions of the channel are shown in conjunction with the structure in Fig. 3 *A*.

To predict conductances Eq. 1 is adapted to use the geometry found by HOLE:

$$G_{\text{macro}}^{-1} = \sum_{z=\text{low}}^{z=\text{high}} \frac{\rho_{\text{bulk}}(c)s}{A(z)}, \tag{2}$$

where the resistivity of the permeant ions (ρ_{bulk}) is regarded as a function of the molar ion concentration c, and the coordinate z is parallel to the channel direction vector. This treatment has similarities to that set out by Kuyucak and Chung (1994) and was first introduced into the HOLE methodology by Sansom and Kerr (1995). The above treatment makes the approximation that the electric field lines running down a pore will be parallel to the channel direction vector, despite deviations from cylindrical geometry in the channel. This is unlikely to prove to be a problem, as the structural models of channels considered here have reasonably uniform geometries and any deviation will on average be represented within the empirically based correction function, discussed below.

It was decided to concentrate on predicting the conductance of channels in potassium chloride solution. KCl was chosen, as it is commonly used in conductance measurements and both ions have an ionic radius close to the van der Waals radius of a water molecule. This has advantages when a solvated model of a narrow channel is being considered. In this case the passage of a potassium or chloride ion can be expected to produce a smaller degree of disruption in comparison to larger or smaller ionic species. Another positive aspect is that potassium and chloride ions have a similar diffusion rate in solution (Hille, 1992). This may be important when considering a channel with cationic or anionic specificity. An experimentally determined value of 0.08 Ωm was used for the resistivity of 1 M KCl (Selley, 1977), and a simple linear concentration dependence was assumed for other concentrations. If no experimental conductivity is available for KCl, a prediction can be made for other ionic species by using the resisitivies given by Robinson and Stokes (1959); in these cases results should be regarded as less certain. To avoid the problems associated with saturation and independence (Hille, 1992), it would be desirable to predict the limiting value of molar conductance at low ion concentrations. At present this is constrained by the experimental observations available, which tend to be for high concentrations.

The above macroscopic treatment would be expected to produce good results if ion channels had a scale that was significantly larger than that of a water molecule/ion. Unfortunately, this is not the case for most biological channels; for example, the gramicidin channel (Arseniev et al., 1985; Ketchem et al., 1993) contains a single file of water molecules, and porins (Cowan et al., 1992) have constrictions around the size of three water molecules side by side. Thus, in general, the conductance of ion channels can be expected to deviate from the value given by our macroscopic approximation (Eq. 2). However, similar arguments hold for the application of the Poisson-Boltzmann equation to electrostatic problems (Warwicker and Watson, 1982; Klapper et al., 1986). Yet, in practice, such methods yield useful results for properties that are difficult to calculate by molecular dynamics techniques.

In this work we aim to compensate for deviations from Eq. 2 by using a correction function. The function will vary with a number of characteristic quantities that can be measured by HOLE for any ion channel model. The parameters of the function will be set by empirically fitting the data for a number of well-characterized ion channel structures (the "learning set"). We define a number c_i for each channel considered:

$$c_i = \frac{G_{\text{macro}}}{G_{\text{exp}}}, \tag{3}$$

where G_{exp} is the experimentally found conductance of the channel and G_{macro} is the macroscopically expected conductance for a reasonable model of the channel, calculated with HOLE and using Eq. 2 for the same ionic species and concentration as used in the experiment. HOLE also calculates the minimum effective radius $R_{\text{min}}^{\text{e}}$ for each structure. Variation with the minimum effective radius was chosen, as it was felt likely that the narrowest part of the channel would be most important in determining both the diffusion rate of ions within the channel and energy barriers to translocation. A correction function $C(R_{\text{min}}^{\text{e}})$ is then fitted to the numbers c_i for the learning set. An additional requirement is that the function should equal unity for the limit of very high radius channels, where the macroscopic approximation (Eq. 2) necessarily holds true.

Given a new ion channel structural model (not in the learning set), a HOLE calculation is made and G_{macro}, $R_{\text{min}}^{\text{e}}$ are found for the structure. The correction function is then used to calculate a predicted value for the conductance of the model:

$$G_{\text{pred}} = \frac{G_{\text{macro}}}{C(R_{\text{min}}^{e})}. \tag{4}$$

In section 2.4, a reparameterization of the method is performed and the use of correction functions with parameters other than the minimum effective radius is considered. With the provisions that a sensible parameterization has been made for the correction function and that the channel considered does not differ in a fundamental manner from those in the learning set, the predicted conductance should be reasonable. The structures used here in parameterization and testing are generally experimentally derived and consequently are representative of the normal "resting" state of the channel, which will generally have water molecules within the central pore. It is therefore preferable that model structures should be produced that include a reasonable representation of solvation within the pore, although all water molecules are automatically excluded from consideration during HOLE calculations.

2.2 Parameterization

Given the limited high-resolution structural information on ion channels available, it was decided to restrict the learning set to the gramicidin channel structure (Ketchem et al., 1993) and the OmpF porin from *Escherichia coli* (Cowan et al., 1992), which will be designated here by its Brookhaven Protein Databank (Bernstein et al., 1977; Abola et al., 1987) pdb code 1omf. These channels were chosen because they have well-characterized, high-resolution, three-dimensional atomic structures from nuclear magnetic resonance methods (Arseniev et al., 1985; Ketchem et al., 1993) and x-ray crystallographic (Cowan et al., 1992) methods (solved at a resolution of 2.4 Å). They also have the advantage that they have different sizes, gramicidin representing a narrow channel in comparison to the much wider porin. In addition, the channels have different architectures. Gramicidin has a β-helical secondary structure, made possible by the alternation of L and D amino acids along the peptide (Andersen, 1984; Woolley and Wallace, 1992). This results in a central pore lined by the amino acid backbone. In contrast, porins have a 16-stranded antiparallel β-barrel topology with an internal loop (L3) folding into the barrel (Cowan et al., 1992), with the channel consequently being lined by amino acid side chains.

As discussed in section 2.1, the capsule option of HOLE (Smart et al., 1993; Smart, 1996), in which the pore dimensions of the channel are characterized by spherocylindrical objects (Fig. 1) as opposed to spheres, was used. The all-atom set of van der Waals radii from AMBER (Weiner et al., 1984) was employed. Results of the application of the method are given in Table 1.

A simple linear functional form was assumed for the correction function:

$$C(R^{e}_{min}, \ldots) = \begin{cases} b - aR^{e}_{min} & \text{when } R^{e}_{min} < (b-1)/a \\ 1 & \text{when } R^{e}_{min} > (b-1)/a. \end{cases} \quad (5)$$

The coefficients a and b were fitted to the data for gramicidin and lomf taken from Table 1. The correction function so determined was included as part of HOLE program and is plotted in Fig. 2. In reparameterization (section 2.4), alternative functional forms and parameters are considered.

TABLE 1 Parameterization: the first-generation correction factor

Structural model	KCl molarity	G_{expt} (pS)	R^{e}_{min} (Å)	G_{macro} (pS)	$c_i = G_{macro}/G_{expt}$
Gramicidin A Ketchem et al. (1993)	0.5	31*	1.28	173.8	5.61
E. coli porin Ompf Cowan et al. (1992)	1	700#	3.90	3485	5.00

*Value from Hladky and Haydon (1972).
#Value given by Benz et al. (1985) is 2.1 nS for 1 M KCl, but following the reasoning of Jap and Wallian (1990) this is for a trimer, so it is divided by 3 here.

2.3 Validation

A literature search was made for well-characterized experimental and model 3D structures of ion channel-forming peptides and proteins. Helical bundle models in which there was an ambiguity in identifying the number of helices corresponding to a particular conductance state were excluded from consideration. The systems considered, the structures of which are compared in Fig. 3, fall into three groups:

(a) High-resolution experimental structures

E. coli phosphoporin 1PhoE x-ray crystallographic structure (pdb code 1pho; Cowan et al., 1992), solved to a 3.0-Å resolution. This molecule, although homologous to the OmpF porin from the same organism (with 63% sequence identity), has distinct structural and conductance properties, showing anionic selectivity (Benz et al., 1985).

The porin from *Rhodobacter capsulatus* solved at a resolution of 1.8 Å (2por; Weiss and Schulz, 1992). This porin is only distantly related to the two *E. coli* porins used, with no detectable sequence similarity.

Maltoporin from *E. coli* solved to a resolution of 3.1 Å (1mal; Schirmer et al., 1995). This molecule, although adopting a β-barrel architecture similar to that of the other porins considered here, has no detectable sequence homology. Furthermore, the β-barrel is composed of 18 as opposed to 16 strands, and there are three loops that fold into the barrel, resulting in a constriction that is narrower than the other porins. The crystal structure, although containing a trimer in the asymmetrical unit, was solved using non-crystallographic symmetry (ncs) constraints. Because part

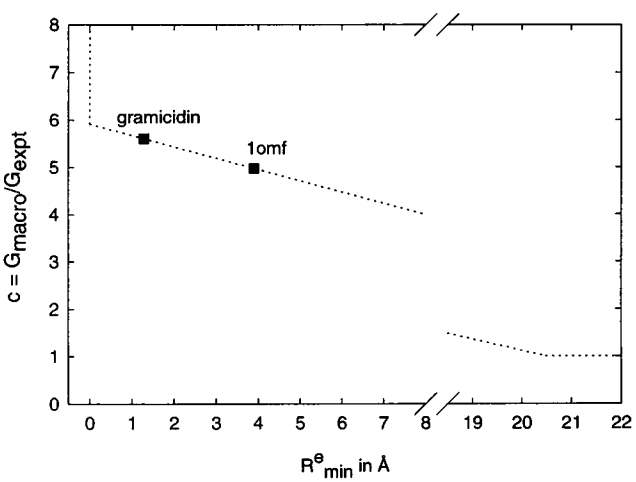

FIGURE 2 The correction function varying in the minimum effective radius (Fig. 1) used in this work.

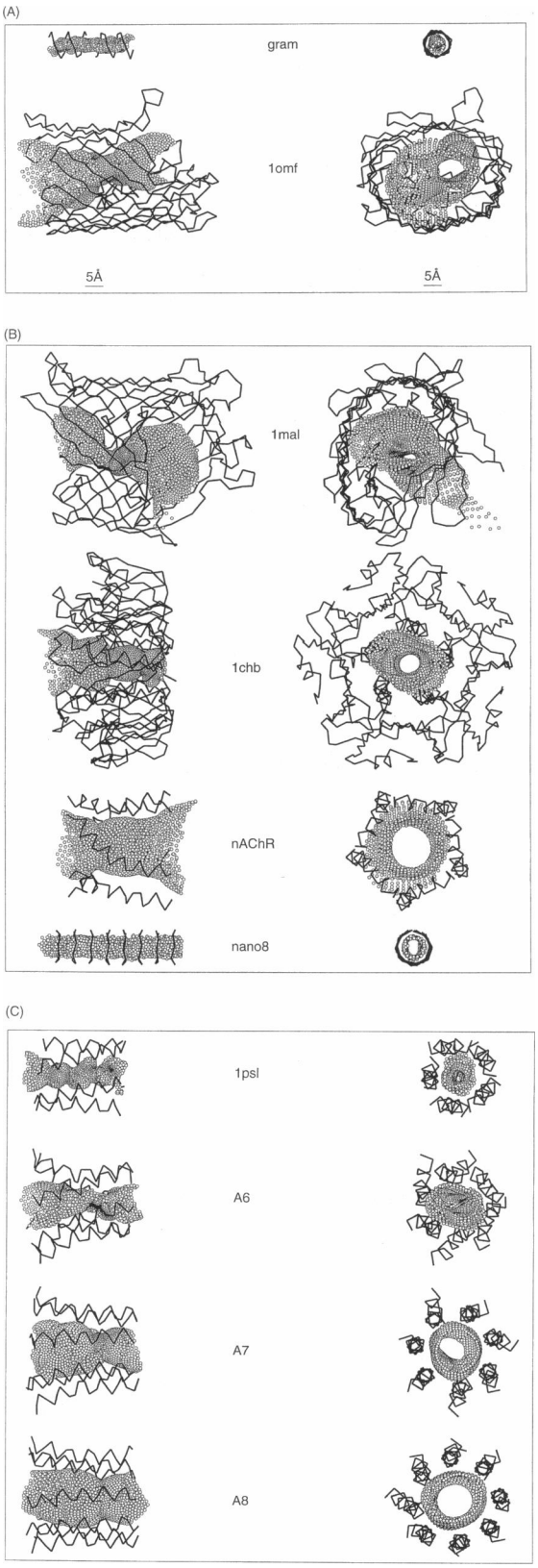

FIGURE 3 The pore dimensions of the ion channel structural models considered here. In all cases the molecule architecture is shown by a Cα trace in conjunction with a dot surface of the internal pore, as calculated by HOLE. For each molecule two views are shown side by side. In the left-hand view the channel direction vector runs across the page, whereas on the right the orthogonal view, down the channel direction vector, is taken. The scale is same in all parts and is illustrated in *A*. (*A*) The two molecules used in the training set. gram, gramicidin A; 1omf, *E. coli* OmpF porin. (*B*) Four members of the experimental and well-characterized model structures. 1mal, maltoporin; 1chb, cholera toxin B-subunit pentamer; nAChR, nicotinic acetylcholine receptor α7, nano8, nanotube forming cyclic octapeptide. In addition to the structures shown, two porins (1pho and 2por) are members of this group. (*C*) Other model structures considered. 1psl, phospholamban; A6, A7, A8, models of distinct conductance states of alamethicin with differing numbers of helices.

of the pore lining comes from a neighboring ncs copy, the full trimer was constructed and considered.

Cholera toxin B subunit x-ray crystallographic structure (1chb; Merritt et al., 1994) determined to a resolution of 2.2 Å. This structure is a pentamer with a central pore formed by α-helices. The intact toxin has a well-demonstrated ability to form channels in lipid bilayers (Tosteson and Tosteson, 1978). This has been shown to be entirely attributable to the presence of the B-subunit (Krasilnikov et al., 1991). It is unclear whether this behavior has any role in its physiological/pathological mechanism of action (Zhang et al., 1995).

(b) Well-characterized model structures

A model built of the self-assembling, nanotube-forming cyclic peptide *cyclo*[-(trp-D-leu)$_3$-gln-D-leu-] reported by Ghadiri and co-authors (Ghadiri et al., 1993, 1994). This structure is composed of a cyclic octapeptide that can form extended tubes by forming a β-sheet-like, hydrogen-bonded stack. The ring is sufficiently rigid that the conformation is essentially unambiguous, as has been confirmed by the crystal structure of a closely related peptide (Ghadiri et al., 1995) and by a detailed molecular dynamics study (Engels et al., 1995). The only factor decided in the modeling was number of stacked rings in the structure. Eight rings were considered, yielding an approximate channel length of 31 Å, which is reasonable in comparison to the typical thickness of a lipid bilayer, (Fettiplace et al., 1971). The structure was built using the program QUANTA (Molecular Simulations, Waltham, MA) and refined with TIC (Smart, 1991).

A model of the pore domain of the nicotinic acetylcholine receptor homopentameric α7 in the open state (nAChRα7) (Sankararamakrishnan et al., 1996). The model was derived from molecular dynamics simulations using restraints derived from 9-Å-resolution cyroelectron microscopy data (Unwin, 1995). Because of the detailed nature of the experimental information that defines the pore dimensions of the channel, this structure can be regarded as well determined.

(c) Other Model structures

Alamethicin bundles. These channels were modeled on the barrel stave hypothesis (Fox and Richards, 1982; Sansom, 1993). The x-ray crystal structure determined by Fox and Richards (1982) was used for individual helices, and bundles with a varying number of helices were constructed using molecular dynamics simulated annealing. The modeling process broadly followed the protocol set out by Kerr

et al. (1994) and Breed et al. (1996) and will be fully described in Breed et al. (1997). The identification of the number of helices in the bundle for each conductance state is based on work conducted by Woolley and co-workers on covalently linked dimers of alamethicin (You et al., 1996).

A model for the transmembrane domain of phospholamban (Adams et al., 1995) (pdb code 1psl). The channel is selective for Ca^{2+} ions, but has measurable activity with potassium chloride. The transmembrane domain channel is known to be formed of a homopentamer (Kovacs et al., 1988) of α-helices (Simmerman et al., 1989). The model (Adams et al., 1995) was based on restrained modeling guided by detailed mutagenesis data and is supported by a variety of spectroscopic data (Ludlam et al., 1996).

The procedure described in section 2.1 was then used to calculate an expected conductance for each channel in potassium chloride solution at the concentration used in the corresponding experiment. All solvent molecules within the structures were excluded from consideration during the calculations. For the systems that were the product of modeling techniques that resulted in multiple structures (simulated annealing and molecular dynamics simulation), the procedure was run on a representative sample of positions and the results were averaged. The results appear in Table 2 and are presented graphically in Fig. 4.

To be able to gauge the overall success of the procedure, we define the factor F fora given prediction:

$$F = \begin{cases} G_{pred}/G_{expt} & \text{if } G_{pred} > G_{expt} \\ G_{expt}/G_{pred} & \text{otherwise.} \end{cases} \quad (6)$$

Thus if a prediction is entirely correct, F is equal to 1, and the larger the value the worse the prediction. This can be seen to be preferable to a simple percentage measure of success, as it is much more of a problem to underestimate the true value G_{expt} by 90% ($F = 9$) than overestimate it by 90% ($F = 1.9$).

A more mathematically rigorous measure of success is provided by the predictive r^2 (Cramer et al., 1988; Head et al., 1996):

$$\begin{aligned} r^2_{pred} &= (SD - press)/SD \\ press &= \sum_{i=1}^{N} (G_{pred,i} - G_{expt,i})^2 \\ SD &= \sum_{i=1}^{N} (\bar{X} - G_{expt,i})^2, \end{aligned} \quad (7)$$

TABLE 2 Assigning a conductance value to structural models of ion channels (first-generation prediction)

System	KCl (M)	G_{exp} (pS)	R^c_{min} (Å)	G_{macro} (pS)	G_{pred} (pS)	Prediction factor F
High-resolution experimental structures:						
Porin (2 por)	1	1100*	4.45	5900	1200	1.11 (over)
Porin (1 pho)	1	600¶	3.39	3200	630	1.05 (over)
Maltoporin (1 mal)	1	160##	2.85	2200	420	2.64 (over)
Cholera toxin B pentamer (1 chb)	0.1	125#	3.24	320	60	1.98 (under)
Well-characterized model structures:						
nAChRα7	0.08**	45**	5.90	400	88	1.96 (over)
nano8	0.5	65§	2.48	330	65	1.00
Other model structures						
Phospho-lamban (1 psl)	0.05	10‖	1.59	37	6.6	1.52 (under)
Alamethicin A5 ($C = 0$)	1	19§§	0.15(0.16)¶¶ 0.83(0.56)	70 (60) 1200 (900)	11 (10) 200 (200)	~‖‖
Alamethicin A6 ($C = 1$)	1M	280§§	1.4 (0.5)¶¶ 1.7 (0.4)	1200 (300) 1700 (700)	220 (50) 320 (130)	1.03 (under)
Alamethicin A7 ($C = 2$)	1M	1300§§	3.3 (0.4)¶¶ 3.7 (0.2)	2800 (400) 3000 (140)	560 (80) 600 (20)	2.25 (under)
Alamethicin A8 ($C = 3$)	1M	2700§§	4.3 (0.5)¶¶ 5.5 (0.2)	3900 (500) 4300 (200)	800 (130) 930 (40)	3.13 (under)

*Value given by Benz and Bauer (1988) is 3.3 nS, but following the reasoning of Jap and Wallian (1990), this is for a trimer, so it is divided by 3 here.
#Krasilnikov et al. (1991).
§Ghadiri et al. (1994).
¶Dargent et al. (1986).
‖Kovacs et al. (1988).
**Value given by Revah et al. (1991) is for 80 mM KF + 5 mM $MgCl_2$, prediction is for this mix using bulk conductivity correction from Robinson and Stokes (1959).
##Benz et al. (1986).
§§Hanke and Boheim (1980).
¶¶Upper figure gives the result for the set of positions that is the output of the simulated annealing process (models are unsolvated). The lower figure is the result for a short solvated molecular dynamics run of a single position. The figures in brackets are the standard deviations found across the set of positions found.
‖‖ No prediction possible.

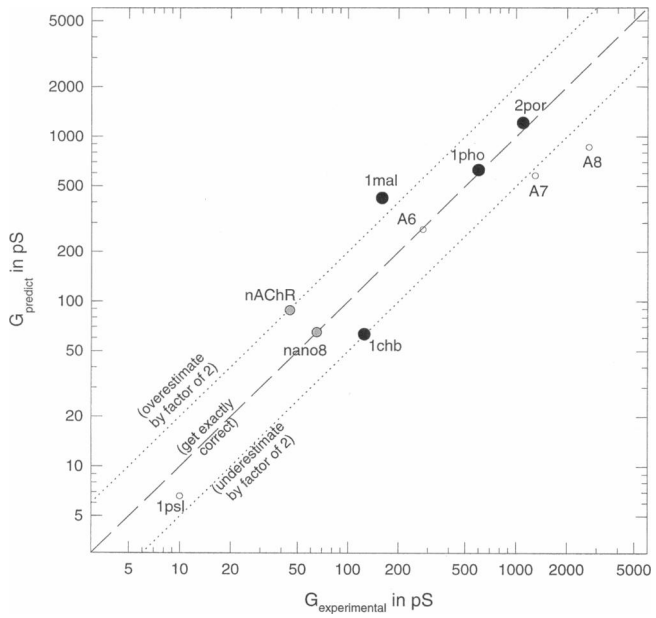

FIGURE 4 Using the first generator prediction process to assign conductances to ion channel atomic structures. Note that the scales use log units. Points marked by filled systems have structures that have been experimentally determined, whereas open points mark structures that are the result of modeling processes. For details of the labels used see text and Fig. 2.

where N is the total number of predictions and $\bar{X}$ is the mean value of the relevant quantity (in this case conductance) for the training set used to parameterize the model. If a prediction is completely successful (so that $G_{pred,i} = G_{expt,i}$ for all cases), then r^2_{pred} will be equal to 1. On the other hand, the naive prediction that the quantity will always be equal to the mean value in the training set will give a r^2_{pred} equal to 0. Thus the better the prediction, the closer r^2_{pred} comes to 1, and the worse the prediction, the lower the quantity becomes. It is possible for an algorithm to produce a value less than 0, indicating no predictive power.

Fig. 2, with Tables 2 and 3, shows that the procedure gives very encouraging results in being able to "predict" the conductance of a channel from three-dimensional coordinates.

The predictions for the two porins (1pho and 2por) and the nanotube-forming cyclic octapeptide (nano8) are essentially correct. For cholera toxin B-subunit pentamer (1chb), maltoporin (1mal), and nAChRα7 results are not quite so good, predictions being off by a factor of ~2. The r^2_{pred} for these six well-characterized systems is 0.90. In comparison,

TABLE 3 Overall performance of the conductance prediction procedure

Systems	Mean prediction factor $\langle F \rangle$	Predictive r^2
Well-characterized systems (a) and (b) (total number 6)	1.62	0.90
All systems (a), (b) and (c) (total number 10)	1.77	0.46

a sophisticated method for predicting the binding affinities of ligands to proteins on the basis of structure (Head et al., 1996) results in a r^2_{pred} between 0.5 and 0.8. In some respects it is surprising that such a crude model performs so well: it would appear that simple steric factors can account for a great part of the differences in absolute conductance between channels. Although predictions are within a mean factor of 1.6, there are outliers, and it is clear that further development will be necessary to meet the hoped-for consistent reliability within a factor of 2.

These results make it possible to start using the procedure as part of a validation process for model channel structures, which are less well-defined by experimental data. A difference greater than a factor of 3 between the predicted and expected values for conductance can be regarded as significant. In this spirit, an examination of the models (c) with less well-characterized structures was undertaken. Phospholamban has an encouraging agreement; the predicted value is well within the hoped-for factor of 2 of the true value. Results for the alamethicin bundles are mixed. For the five-helix bundle A5, which is identified with the low conductance ($C = 0$) state, the great spread of results between the initial ensemble and the molecular dynamics run do not allow the prediction of a value. For the A6, six helix bundle results are good. However, the seven (A7) and eight (A8) helix bundles are underpredicted by factors of 2 and 3, respectively. These differences are on the edge of the margin of error of the prediction routine, but the effect may be because the structures are too compact, resulting in a narrow pore. Alternatively, it may, for example, reflect the effects of the lipid headgroups (not included in the simulations) on the dimensions of the C-terminal mouth of the pore. These alamethicin model structures are also considered when analyzing the effect of nonelectrolytes on conductance, in section 3.3, where similar conclusions are drawn. Although the overall measures of the predictive ability of the HOLE method are made worse by the inclusion of all of the model structures (Table 3), they are still quite reasonable, and it should be remembered that the deviations could be contributed to by uncertainties in the structures.

2.4 Reparameterization

The prediction technique set out in the previous sections relied on using a correction function with an assumed dependence on the minimum radius of the channel. Given all the results obtained for the molecules with well-defined structures, it is possible to ask whether this assumption was reasonable and whether a better choice can be made for future predictions. The answer can be obtained by reparameterizing the correction function. The six high-resolution experimental structures and two well-characterized model structures were used as the training set. The HOLE program was adapted so as to measure a number of characteristic quantities for any channel structure (for example, minimum effective radius, length, or average proportion of pore sur-

face closest to oxygen/nitrogen atoms). For each quantity ξ, a number of alternative functional forms were tried for a correction function:

$$C(\xi) = \begin{cases} b + a\xi & \text{linear or} \\ 1/(b + a\xi) & \text{inverse linear or} \\ b + a\xi + d\xi^2 & \text{parabolic or} \\ 1/(b + a\xi + d\xi^2) & \text{inverse parabolic.} \end{cases} \quad (8)$$

A fitting procedure using a simple Monte Carlo annealing procedure (with multiple restarts) to minimize the rms prediction factor for the training set was then applied for each of the four alternative correction functions. Results of the reparameterization are shown in Table 4 in comparison to a simple constant correction (the uppermost Eq. 8, with a set to 0). The electrostatic potential calculations performed were simple, with a uniform dielectric constant of 1 being used and only the effect of uncompensated formal charges of a system being considered. Two calculations were performed in each case, one in which histidine residues were treated as uncharged and an alternative in which they were assigned a charge of +1.

Most noteworthy in many respects are the quantities that provided only small improvements over a constant correction factor. The minimum effective radius is such a quantity. Although the initial parameterization on just two systems proved to be serendipitously close to the optimum for the full set (Fig. 5 *A*), there is really no overall tendency in the data that indicates a variation in C with this quantity. This means that it is a poor variable to choose to apply a correction function. Indeed, it gives no significant improvement in fit in comparison to a constant correction for all systems (Table 4). The same is true for the aspect ratio, tortuosity of the channel, the molarity of the solution used in the experiment, the predicted macroscopic conductance, and the proportion of the channel surface surrounded by oxygen/nitrogen atoms. These quantities can be ruled out for future consideration.

Significant improvements between the predicted and experimental conductance were found for two quantities: the length of the channel and its net overall charge. Both the average electrostatic potential and the simple difference between the number of basic and acidic residues can be seen to be measures of the overall charge. In many respects it would be easier to rationalize a variation found in one of the alternative quantities, but the data seem clear. The best-fit correction functions found are shown as Fig. 5, *B* and *C*. Fig. 5 *D* shows

TABLE 4 Reparameterization of the conductance prediction procedure

Quantity	Linear fit	RMSF inverse linear	RMSF parabolic	RMSF inverse parabolic
fn form	$C(\xi) = b+a\xi$	$C(\xi) = 1/(b+a\xi)$	$C(\xi) = b+a\xi+d\xi^2$	$C(\xi) = 1/(b+a\xi+d\xi^2)$
Number of fitted params	2	2	3	3
Length *LE*	0.18	**0.24**	0.22	0.25
1/*LE*	0.14	0.18	0.17	0.23
LE^2	0.12	0.15	0.24	0.32
Minimum effective radius *ME*	0.00	0.00	0.04	0.05
Aspect ratio = *LE/MR*	0.07	0.09	0.12	0.19
Distance along centerline *DA*	0.17	0.23	0.23	0.25
Tortuosity = *DA/LE*	0.01	0.02	0.08	0.18
Ionic molarity *MO*	0.03	0.03	0.03	0.03
G_{macro} *GM*	0.00	0.00	0.04	0.04
Molal G_{macro} = *GM/MO*	0.00	0.00	0.00	0.00
No. basic residues *NB* (excl his)	0.04	0.05	0.18	0.13
No. acid residues *NA*	0.00	0.00	0.05	0.08
NB-NA (excl his)	0.14	0.27	0.23	0.28
NB-NA (incl his)	0.12	0.16	0.18	0.18
Avg electrostatic potential (no his) *POT*	**0.26**	0.22	0.26	0.23
Avg electrostatic potential (+his)	0.23	0.19	0.23	0.24
Electrostatic potential barrier (no his)	0.00	0.00	0.01	0.01
Mean proportion perim bounded by oxygen/nitrogen	0.02	0.02	0.03	0.06
Mean proportion perim bounded by acid/base (PAB)	0.03	0.23	0.24	0.26
Combined quantities				
PAB/LE	0.13	0.35	0.26	0.35
*PAB*LE*	0.01	0.01	0.03	0.03
POT/LE	0.20	**0.36**	0.21	0.36
*POT*LE*	0.30	0.28	0.30	0.28
(*NB-NA*)/*LE* (excl his)	0.10	0.17	0.22	0.25
(*NB-NA*)**LE* (excl his)	0.19	0.17	0.21	0.17

In each case the number given is the improvement in the root-mean-square prediction factor for the test set over a simple constant correction factor (rms F = 1.5376, best factor b = 5.594). The grey boxes mark functions that are plotted in Fig. 5.

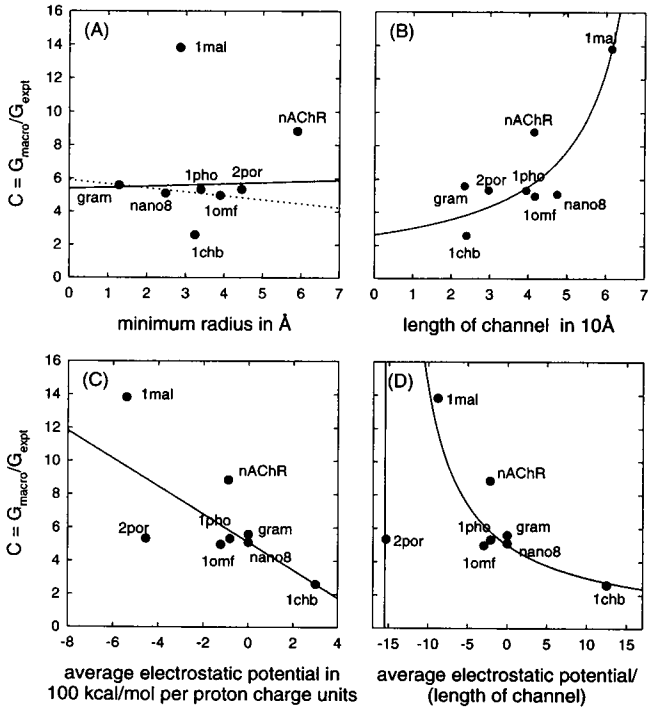

FIGURE 5 Work to reparameterize the correction function. In each case the deviation between the macroscopically and the experimental conductance c_i (Eq. 3) is plotted against a characteristic measured quantity for each channel. In *A* variation with the minimum effective radius of the channel is considered. The solid line shows the best-fit (for prediction) correction function, and the dashed line shows in comparison the first-generation correction function. (*B* and *C*) More successful correction functions in the length of channel and average electrostatic potential. (*D*) A hazard in such a fitting procedure, where the correction function has an asymptote in the range, making it unsuitable for making predictions.

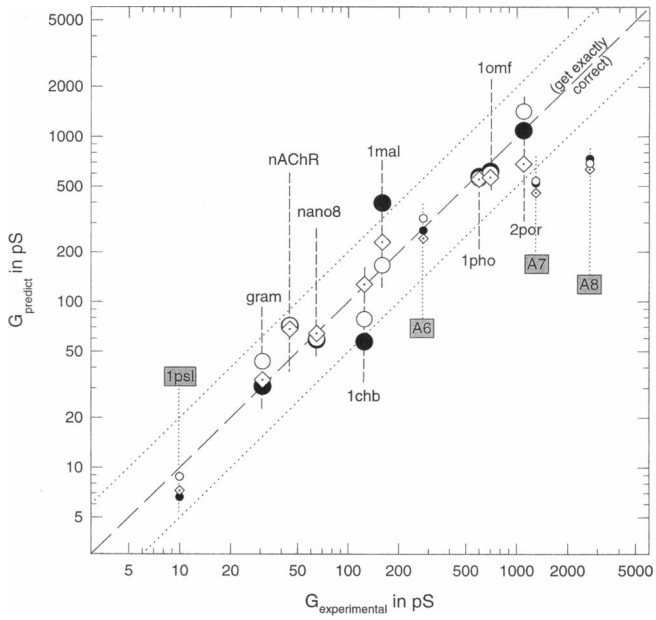

FIGURE 6 The fit between the data used in parameterizing the 2nd-generation correction functions and the final results. Points marked by large filled circles mark the best fit available for a constant (one-parameter) correction function. The large open circles mark the results obtained using an inverse linear fit on the length of the channels. Large diamonds show the fit that can be obtained using a linear correction function on average electrostatic potential. The smaller points (labeled within boxes) show the results obtained for systems with less certain structures that were not included in the fitting procedure.

that it is important to check that the correction has a reasonable form. Although the combination of the average electrostatic potential and length gives the best fit between the data and the function (Table 4), the presence of an asymptote in the range of the fit clearly precludes its use in practice.

As the length and average electrostatic potential yield similar fits between the observed data and the fitted form, the HOLE program has been adapted to produce estimates based on correction functions of both quantities as well as a simple constant correction (which is close to the original parameterization). An advantage in giving three estimates of conductance is that the spread between them gives an immediate impression of the precision of the estimate to the user. The very slight improvements yielded by parabolic functions where not felt to justify the introduction of an additional parameter to be fixed. The fit between the data used to reparameterize the prediction and the final results is shown in Fig. 6.

Although there are insufficient data to be able to properly check the reparameterization, the results on the phospholamban channel and the three distinct conductance states of alamethicin are about as good as the original parameterization (Fig. 6).

2.5 Prediction of unknown quantities

In many ways the best test of any method is to make genuine predictions for unknown quantities. The is done for the porin from *Rhodopseudomonas blastica*, the crystal structure of which has been reported (1prn; Kreusch and Schulz, 1994), but for which we were unable to find any conductance data. Also considered is a 10-residue analog of the 8-residue cyclic L-D repeating peptide that forms nanotubes. This peptide has been synthesized (Granja and Ghadiri, 1994), and its conductance properties have been measured but have yet to be reported. A model for this peptide was constructed in an analogous manner to its 8-residue analog. Once again, an assembly of eight stacked rings was considered. Results for two molecules are given in Table 5.

Clearly, we would be most interested in any experimental measurements for these quantities and in making predictions in similar circumstances.

2.6 Discussion

As the prediction technique developed involves empirical fitting, results should be much better for systems that are

TABLE 5 Predicted conductances for systems without reported experimental values

System	Constant correction	Predicted conductance in pS using 1 M KCl: Correction on length	Correction on avg. potential	Overall prediction*
nano10	220	210	250	230
porin 1prn	690	550	480	570

*The overall prediction is the simple average of the three individual predictions.

similar to those in the "learning set" than for structures with unrepresented major features. This feature is inherent to any such procedure—interpolation is always more reliable than extrapolation. For the first-generation predictor, results for the two porins and nanotube-forming cyclic octapeptide are the best, as these systems are similar in nature to the porin and gramicidin channel that make up the learning set. However, good results were obtained for all of the systems tested, and it is hoped that future predictions for systems with similar architectures (α-helical bundles, β-barrels, and β-helices formed by L-D repeating peptides) will yield reasonable results. However, as the method is still in its infancy, users are cautioned not to read too much significance into any one result.

The wide deviation between the expected conductance from the uncorrected macroscopic model (G_{macro}) considered and the experimental conductance is notable for all systems. This can be most easily demonstrated by examining the value of the correction factor c_i (Eq. 3), as shown in Fig. 5.

The correction factor has a wide range, from 2.5 to 14, with a clustering around 5. A number of complementary factors could contribute to the high value:

The diffusion coefficient of an ion within a confined pore can be expected to be markedly reduced in comparison to that found in free solution. A simplistic picture can be obtained by considering the mean free path length of an ion, which is directly related to the diffusion coefficient (by the Einstein equation). In the confined space within a pore the mean free path length can be expected to be much reduced (particularly in directions orthogonal to the channel axis). A number of authors (Engels et al., 1995; Roux, 1995; Breed et al., 1996) have calculated that the self-diffusion coefficient for water molecules within a channel are reduced by factor of a magnitude similar to that of the correction factor.

Any free energy barriers significantly larger than those for normal ionic diffusion can be expected to drastically alter the conduction rate. However, experience suggests that even for narrow channels such as gramicidin such barriers may be small. The activation energy for ionic motion through gramicidin is similar to that for diffusion of an ion through bulk solution (Hladky and Haydon, 1972).

The reparameterization work (section 2.4) suggests that longer channels have a tendency to have a higher C factor than shorter channels (Fig. 3 *B*). Syganow and von Kitzing (1995) have noted in theoretical studies that channels that are "long" tend to have a different conduction mechanism from "short" channels, which leads to a higher effective resistance and thus a higher C factor. Another tendency is that channels that carry an overall positive charge tend to have a higher C than those that are negatively charged. The effect of charge may be linked to the ionic selectivity of the channels. However, further data will be needed to show conclusively that these effects are real. More detailed explanations may become apparent by linking microscopic simulation within the prediction methodology (see section 2.7).

It is worth considering the relevance of the data shown in Fig. 5 to predictions from conductance data of the pore dimensions of a channel in terms of a cylindrical model. The high value of the correction function can alternatively be thought of as a reduction in the effective conductivity of the ionic species within the channel. Before high-resolution crystal structures were obtained for porins, a number of workers made such predictions (reviewed by Jap and Walian, 1990), making the seemingly reasonable assumption that the conductivity of ionic solutions inside the channel was the same as the bulk conductivity. The resultant radii were considerably smaller (2.4–2.7 Å) than those obtained by consideration of solute exclusion (at around 4.2 Å). Analysis by HOLE of the x-ray crystal structures subsequently determined reveals a minimum effective radius of around 3.8 Å (Tables 1 and 2), showing that the solute exclusion measurements resulted in correct predictions. The success, on a wide range of channels, of the empirically corrected conductance prediction technique set out here means that any future prediction of effective pore dimensions from conductance data should take the correction factor C into account (a reasonable assumption would be to divide the bulk conductivity by a factor of 5).

2.7 Development prospects

The method set out here relies on using simple, empirically fitted correction functions to improve a prediction based on a macroscopic treatment of the problem. This approach has many advantages, including tractability; the calculations take only a small amount of cpu and could be easily undertaken by nonspecialists. In terms of the future progress of the methodology set out here, more well-characterized ion channel structures would be extremely useful. However, to achieve markedly improved predictive power for this methodology, a consistent set of conductance measurements for the channels considered would be particularly beneficial. This would avoid the errors inherent in comparing measurements made by distinct techniques and crucially avoid the use of different ionic concentrations and species. The use of a low ionic concentration in such a study would be desirable, as effects such as saturation and ionic flux coupling (Hille, 1992), which occur at high concentrations, could be avoided.

It may be possible to improve the predictions by using simulation methods to avoid the necessity of using empiri-

cally derived correction factors. Such methods should be capable of predicting specific deviations from the norm for individual channels. In particular, it may be useful to include in the correction process a calculation of the self-diffusion coefficient of water molecules in the channel, using the methodology set out by Breed et al. (1996), which has already yielded results which, as already discussed, indicate a deviation between the value of this parameter between the normal solution value and that found in the channel, which is similar to the values c_i found. Using relatively short simulation times, it is possible to find the self-diffusion coefficient $D_s(z)$ as a function of z, the coordinate along channel direction vector. By assuming that the diffusion coefficient of an ion within the pore varies by the same effect, Eq. 2 could be adapted to directly give a predicted conductance:

$$G_{\text{pred}}^{-1} = \sum_{z=\text{low}}^{z=\text{high}} \frac{\rho_{\text{bulk}}(c) D_s(z)}{D_s(bulk)} \frac{s}{A(z)}, \tag{9}$$

where $D_s(bulk)$ is the value for the self-diffusion coefficient derived in a manner similar to that of a simulation of an isolated box of water molecules.

In many ways a direct calculation of the diffusion coefficient of the ion within the channel (Lynden-Bell and Rasaiah, 1996) would be even better, although this may prove to be more computationally challenging. In addition, an estimation of the potential energy barrier to ion passage could also be usefully included. This could be calculated by using a Poisson-Boltzmann equation-based method—using a dielectric model for the solvent and lipid bilayer or by generalizing the approach of Dorman et al. (1996). Such techniques have proved to be useful in explaining the ion selectivity of porins (Karshikoff et al., 1994), gramicidin (Dorman et al., 1996), and nicotinic acetylcholine receptor (Sankararamakrishnan et al., 1996). However, it may be useful to include the steric effects on the ion and allow the channel to move during the simulated translocation. The path energy minimization protocol (Smart, 1994, 1995; Smart and Goodfellow, 1995) would be ideally suited to such an application. If these methods could predict the variations of the value of C for maltoporin, cholera toxin B-subunit pentamer, and nAChRα7, a more powerful prediction method could result. Work is planned to explore this area. An important factor to be borne in mind when introducing more complicated protocols is to keep the overall prediction technique tractable in terms of computational time and reasonable ease of use.

3. ANALYZING THE EFFECT OF NONELECTROLYTES ON CHANNEL CONDUCTANCE

3.1 Background

Measurements of the effect of the addition of soluble nonelectrolytes to the medium in conductance experiments can be used to gain information on the pore dimensions of a channel (Krasilnikov et al., 1992). The standard experiment measures the effect of the presence of high concentrations (15% or 20%) of neutral polymers such as polyethylene glycol (PEG) on the conductance of the ion channel of interest. The variation of conductance is measured as a function of the molecular weight of PEG (at a constant weight fraction). In bulk solution the conductivity of ionic solutions is reduced in the presence of PEG. This is due to the increase in the viscosity of the solution, with a consequent decrease in the ionic diffusion coefficients and conductivity. Krasilnikov et al. (1992) showed that this reduction is broadly independent of the molecular weight of the PEG used, provided a constant weight fraction is maintained.

When a PEG with a low molecular weight is added to the medium of a channel experiment, the conductance will drop by the same factor as the bulk conductivity (the situation in Fig. 7 *A*). However, as the size of the PEG added is increased, there is a recovery in conductance as the nonelectrolyte is progressively excluded from the channel interior (Fig. 7, *B* and *C*). This exclusion has been linked to the hydrodynamic radius of the polymer. Polymers such as PEG have been shown to be approximately spherical in solution (Rempp, 1957; Krasilnikov et al., 1992). The hydrodynamic radius is obtained from the diffusion coefficients of the polymers in solution (Kuga, 1981) and is found to vary with the square root of the molecular weight of the polymer. Different workers take distinct approaches to obtaining a "characteristic radius" of a particular channel, from the

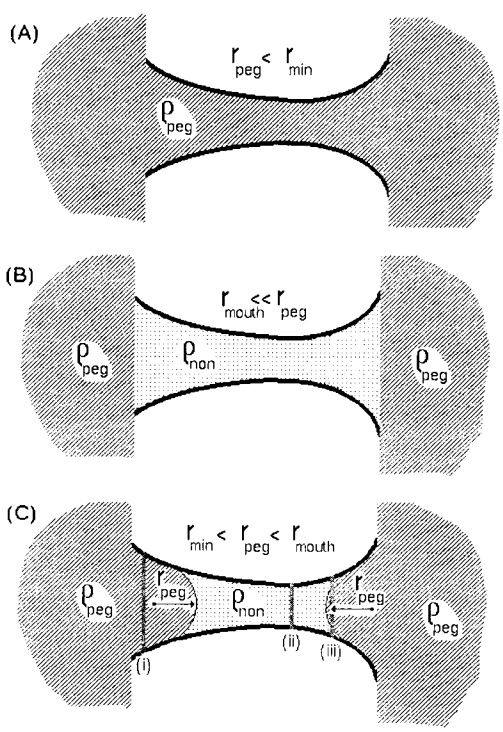

FIGURE 7 A schematic diagram explaining the use of HOLE in analyzing the effect of nonelectrolytes on channel conductance (for further details see text).

measured conductance profile. Some take the 50% effect radius (Bezrukov and Vodyanoy, 1993; Korchev et al., 1995). In contrast, Krasilnikov et al. (1991, 1992) prefer to fit two straight lines to the data: one when the conductance plateaus at high radius/molecular weight and another at lower radius. The characteristic radius is taken as the intersection point between these lines. Needless to say, these approaches yield quite different values.

When very large molecular weight PEGs are added to the conductance medium, there is normally an increase in conductance compared to the PEG-free measurement. Such behavior has been observed for *Vibrio cholera* cytolysin (Krasilnikov et al., 1992) and for three different conductance states of the alamethicin channel (Bezrukov and Vodyanoy, 1993). For *Staphylococcus aureus* α-toxin, Krasilnikov et al. (1992) observe such an increase, whereas Korchev et al. (1995) report a conductance equal to that of the polymer-free situation. An explanation for the increases has been offered by Krasilnikov et al. (1992) and Bezrukov and Vodyanoy (1993). This is that PEG is hydroscopic—as the polymer is excluded from the interior of the channel, the water activity of the solution is increased in this space and the conductivity of the permeant ions consequently increases. This effect can also be shown to occur in bulk solutions using a sodium electrode. Bezrukov and Vodyanoy (1993) show how such measurements can be linked to access resistance considerations and a effective end radius can be assigned to a channel. This is because although the polymer is excluded from the interior of the channel, it is still present at the approach to both mouths (Fig. 7 *C*). These authors also show that similar results can be obtained using nonhydroscopic polymers such as dextrans. This is important, as it reduces the possibility that specific interactions between the polymer and ion channel could affect the result.

In the work presented here, we show how the results of the conductance experiments can be linked to the three-dimensional structure of channels using a simple model and data obtained by the HOLE program (Smart et al., 1993; Smart, 1996). An aim of the work is to find out whether the dimensions obtained by nonelectrolyte experiments can be correlated with those found in three-dimensional structures. A description of the theory behind the application is first given, followed by applications to the x-ray structure of cholera toxin B-subunit (Merritt et al., 1994) and models for different conductance states of the alamethicin channel.

3.2 Theory

In this section we intend to calculate the expected conductance ratio (to the polymer free situation) for a channel structure with PEGs of varying molecular weight/radius. The approach is inspired by the model adopted by experimental groups (Krasilnikov et al., 1992; Bezrukov and Vodyanoy, 1993). PEGs are treated as spheres with a characteristic radius (dependent on molecular weight). In a similar manner to that set out in section 2, a HOLE run is used to delimit the pore of the structural model of the channel. This is divided into regions that are accessible to a sphere of the radius of interest and the complement (see Fig. 7 *B*). The former region is assigned a conductivity that has a ratio of Θ_{PEG} to the polymer-free conductivity. Similarly, the latter (inaccessible) part is assigned a conductivity ratio Θ_{NON}. These are the only parameters that enter into the calculation and are set to experimentally measured values for bulk solutions. Note that in contrast to the work set out in section 2, this analysis does not require any empirical fitting. The calculation is ab initio; only the structure and these two experimentally measured solution parameters are needed. For 15% PEG (wt/wt), Θ_{PEG} has been measured to be 0.61 and Θ_{NON} to be 1.14 (Bezrukov and Vodyanoy, 1993).

Equation 1 is adapted to deal with the case of a channel with variable radius (depending on the coordinate along the channel vector z, as determined by HOLE), the inverse conductance for a channel being given by

$$G^{-1} = \sum_{z=zlow}^{z=zhigh} \frac{\rho\, s}{\pi r(z)^2} + \frac{\rho}{4r(zlow)} + \frac{\rho}{4r(zhigh)}, \quad (10)$$

where s is the width of the slabs being considered. The two last terms represent access resistance, where $r(zlow)$ and $r(zhigh)$ are pore radii at the end of the channel (see below for the definition of these quantities in this work). The approach is similar to that in section 2, except that access resistance is of importance here. As the concern of this section is to find the effect of introducing nonelectrolyte polymers on a given channel, the absolute value for conductance is not important. What matters is the ratio of conductance with a particular polymer present to that without (all other conditions being kept fixed). For this reason, considerations of empirically based corrections as introduced in section 2 are not relevant.

Equation 10 must be adapted to give the conductance ratio for a channel where the conducting medium is split, as shown in Fig. 7 *B*:

$$\left[\frac{G_{PEG}(R_{PEG})}{G_{FREE}}\right]^{-1} = N_{PEG}\left\{\sum_{\substack{z=zlow \\ \text{where} \\ r>R_{PEG}}}^{z=zhigh} \frac{s}{\pi r(z)^2} + \frac{1}{4r(zlow)} + \frac{1}{4r(zhigh)}\right\} + N_{NON}\sum_{\substack{z=zlow \\ \text{where} \\ r<R_{PEG} \\ \text{and Aacc}=0}}^{z=zhigh} \frac{s}{\pi r(z)^2} + \sum_{\substack{z=zlow \\ \text{where} \\ r<RPEG \\ \text{and Aacc}\neq 0}}^{z=zhigh} \frac{Y_{PEG}Y_{NON}}{Y_{PEG}+Y_{NON}}. \quad (11)$$

The first term represents the contribution to the resistance by slabs that are filled with PEG (marked (i) in Fig. 7 *B*) and the access resistance of the two ends of channel (this space is always accessible regardless of the value of R_{PEG}). The

factor N_{PEG} is given by

$$N_{PEG} = \left[\Theta_{PEG} \left\{ \sum_{z=zlow}^{z=zhigh} \frac{s}{\pi r(z)^2} + \frac{1}{4r(zlow)} + \frac{1}{4r(zhigh)} \right\} \right]^{-1}. \quad (12)$$

This means that when R_{PEG} is smaller than the minimum radius of the channel (i.e., r is always more than R_{PEG}), Eq. 11 yields the result $G_{PEG}/G_{FREE} = \Theta_{PEG}$, i.e., the conductance of the channel is reduced by the same factor as the bulk conductivity.

The second term represents the resistance of slabs that are completely inaccessible to the polymer sphere, like the section marked (ii) in Fig. 7 *B*. The normalization factor in this case is defined in a manner similar to that of Eq. 10:

$$N_{NON} = \left[\Theta_{NON} \left\{ \sum_{z=zlow}^{z=zhigh} \frac{s}{\pi r(z)^2} + \frac{1}{4r(zlow)} + \frac{1}{4r(zhigh)} \right\} \right]^{-1}. \quad (13)$$

The last term in Eq. 11 represents the resistance of slabs that are partly occupied by PEG and partly not, as indicated by (iii) in Fig. 7 *B*. A_{acc} is the area accessible to PEG. For each slab the term represents the resistance of the two parts acting in parallel:

$$Y_{NON} = N_{NON} \frac{s}{\pi r(z)^2 - A_{acc}(z)}, \quad Y_{PEG} = N_{PEG} \frac{s}{A_{acc}(z)}. \quad (14)$$

At large polymer radii Eq. 11 tends to the limit

$$\left[\frac{G_{PEG}}{G_{FREE}}\right]^{-1} = N_{PEG}\left\{\frac{1}{4r(zlow)} + \frac{1}{4r(zhigh)}\right\} + N_{NON} \sum_{z=zlow}^{z=zhigh} \frac{s}{\pi r(z)^2}. \quad (15)$$

This has the consequence that the limit depends on the ratio between the access resistance and the channel resistance. As the access resistance dominates (the second term tends to zero), the conductance ratio tends to Θ_{PEG}. In the opposite case, when channel resistance dominates and the first term tends to zero, the ratio tends to Θ_{NON}. Thus in the limit of large polymer molecular weight the conductance ratio can take any value between Θ_{PEG} (less than 1) and Θ_{NON} (greater than 1 for hydroscopic polymers such as PEG). If the limit is equal to 1, the increase due to channel resistance is offset by the decrease due to access resistance.

The above treatment has been implemented in HOLE. Some adaptations to the standard procedure are required. For ease of calculation, a spherical probe is used (rather than a spherocylinder). Instead of halting a run when the pore radius reaches a defined limit, it is necessary to define "end radii" at each side of the channel ($r(zlow)$ and $r(zhigh)$ in Eq. 11). The ends of the channel were defined by finding the coordinates of all atoms along the channel vector and taking the extrema. The HOLE run was halted at these ends. To correctly work out the asymptotic behavior of the conductance curve, it is necessary to find the part accessible to PEG from points outside the channel. So at the end of the run, a large number of additional points outside the channel are added for this purpose. The calculation does not significantly increase the cpu cost of a HOLE run—a typical application takes under 10 min on a modern workstation.

3.3 Applications

At present, the only channel-forming protein for which both PEG effect data and a high-resolution three-dimensional experimental structure are available is the cholera toxin B-subunit pentamer. The intact cholera toxin is a heterohexamer AB_5 with a single A-subunit complexed to a pentameric ring of B-subunits, as shown in Fig. 3 *B*. Structures of the hexamer show that the intact complex the central "donut hole" formed by the B-subunits is filled with the A2 α-helix from the A-subunit. However, the B-subunits form a stable complex separately with the central hole unfilled, as revealed by high-resolution x-ray structures recently solved independently by two groups (Merritt et al., 1994; Zhang et al., 1995). Krasilnikov et al. (1991) showed that the B_5 pentamer was able to form ion channels in artificial membranes at low pH. Furthermore, they characterized these channels by polymer exclusion experiments, obtaining a characteristic radius of 10.5 Å.

The HOLE-based procedure, described in section 3.2, was applied to the x-ray crystal structure solved by Merritt et al. (1994) (obtained from the Brookhaven protein databank, code 1chb). Amber van der Waals radii (Weiner et al., 1984) were used in the calculation. The polymer exclusion experiments were carried out using 20% PEG. The value for the reduction in bulk conductivity in the presence of the nonelectrolyte (Θ_{PEG}) was taken as 0.54 (measured from solution data presented by Krasilnikov et al., 1991). The value for the parameter Θ_{NON} (the increase in bulk conductivity in solutions that are separated from PEG) was taken as 1.18, as quoted by Bezrukov and Vodyanoy (1993). The expected conductance profile on the basis of the crystal structure and the HOLE-based procedure are shown in Fig. 8.

Comparison between the theoretically expected and experimental results shows a very encouraging agreement. The expected result goes through all of experimental error bars. In particular, the initial rising part of the curve is well represented. Considering the simplicity of the model and the very different origins of pore radius and the hydrodynamic radius of the polymer, the level of agreement may be felicitous. Only comparison between experimental and expected results for other ion channels with well-characterized experimental structures will reveal whether this is the case.

An important point to be appreciated from Fig. 8 is that to correctly gauge the asymptotic values of the conductance ratio one must perform experiments with PEGs of high

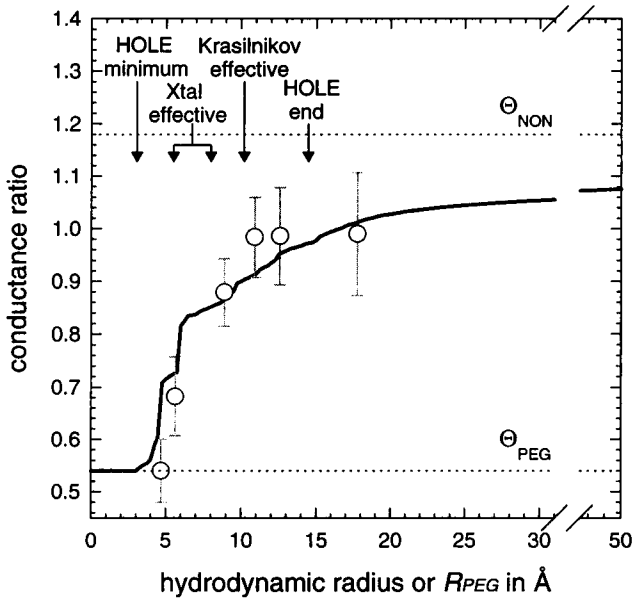

FIGURE 8 The application of the HOLE-based procedure to predict the effect of 20% PEG on the conductance of cholera toxin B-subunit x-ray crystal structure solved by Merritt et al. (1994). The thick solid line shows the expected result. The points marked by circles and error bars are the experimentally measured data reported by Krasilnikov et al. (1991) (taken from that publication using a STOE ratchet film measuring device). The dotted lines mark the values of Θ_{PEG} and Θ_{NON} for 20% PEG solutions. Arrows mark the effective radii quoted by various authors for the system (for further details see text).

molecular weights. The final point in the experiment of Krasilnikov et al. (1991), which did not aim to determine the asymptotic ratio, used a molecular weight of 4000. The expected result at this radius is only 1.01, compared to the asymptotic ratio of 1.08.

It is instructive to compare the effective radii quoted for cholera toxin B-subunit from a number of sources (Krasilnikov et al., 1991; Zhang et al., 1995). Zhang et al. (1995) pointed to the discrepancy between the radii they estimated from their high-resolution crystal structure (from 5.5 to 8 Å) and the characteristic radii interpreted by Krasilnikov et al. (1991) from polymer exclusion experiments (11.5 Å). They postulated that the discrepancy could be accounted for by "widening of the pore after membrane attachment." This process could have implications for the translocation of the A-subunit through the lipid bilayer (possibly in an unfolded form). The work set out here shows that in fact the polymer exclusion experiments and crystallographic data are entirely consistent, and therefore such a process is unlikely to occur. The source of the difficulty in comparing such interpretations is that many workers seem to assume that ion channels have a single characteristic radius, adopting an essentially cylindrical geometry. In reality, channels normally have more complex internal geometries (Fig. 2). Fig. 8 shows how the polymer exclusion data are strongly indicative of this; both the theoretical curve and the experimental data start to rise around the HOLE minimum radius and begin to settle down to their asymptotic values at the HOLE end radius.

Encouraged by the application of the procedure to cholera toxin B-subunit, further work was undertaken on three distinct conductance states of the alamethicin channel. Polymer exclusion data for this system has been measured by Bezrukov and Vodyanoy (1993). As discussed in section 2, atomistic models for each of the conductance states based on the barrel stave hypothesis have been formulated by Breed et al. (1997). The expected conduction ratio graph on the basis of these models is shown in Fig. 9. The application was similar to that for cholera toxin B-subunit pentamer, with the exception that Θ_{PEG} was set to 0.61 and Θ_{NON} to 1.14, the values for 15% PEG given by Bezrukov and Vodyanoy (1993).

In this case the agreement between the expected result based on the model structure and the experimentally deter-

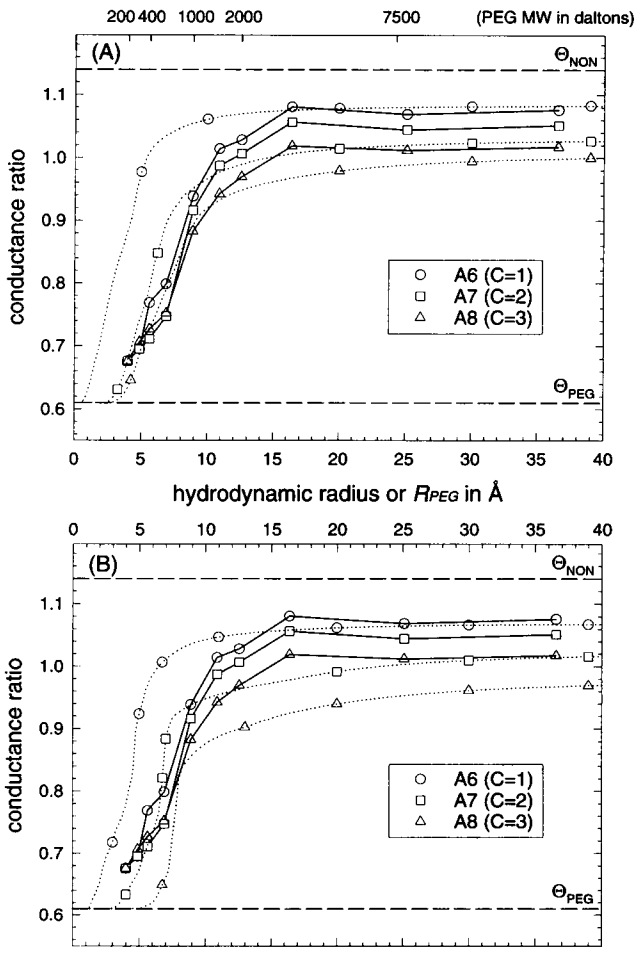

FIGURE 9 The application of the HOLE-based procedure to predict the effect of 15% PEG on the conductance of three different conductance states of the alamethicin channel. Solid lines mark the experimental results given by Bezrukov and Vodyanoy (1993). Dotted lines mark the results obtained from models provided by Breed and Sansom. Alamethicin conductance state 1 is identified with a six-helix bundle, 2 with seven helices, and 3 with an octamer, as discussed in section 2.2. (*A*) The average result for the simulated annealing ensemble; (*B*) for a solvated molecular dynamics run.

mined profile is reasonable. For the hexameric bundle the initial rise in the profile occurs at too short a radius, although the asymptotic value at large radius is well predicted. For the seven- and eight-helix bundles the initial rise in the curve is quite well represented, but the asymptotic values are somewhat underpredicted. In all cases the result from the ensemble of structures that results from the initial simulated annealing part of the modeling process is better than that resulting from the final solvated molecular dynamics run. A possible explanation of these phenomena is that the seven- and eight-helix bundle models are not sufficiently wide. Credence can be added to this idea by directly calculating the end radii calculated for the different states from the model structures. These are compared in Table 6 to those derived from polymer exclusion data by Bezrukov and Vodyanoy (1993), using the absolute conductance and asymptotic ratio. The six-helix bundle appears to be in the correct range, but the seven- and eight-helix cases, although having the correct tendency, are slightly too small. These observations tie in well with the results in predicting the absolute conductances of the models set out in section 2.3 (Fig. 4 and Table 2).

3.4 Discussion

The polymer exclusion method presents an attractive means of deriving information on the pore dimensions of ion channels by using simple conductance measurements. However, to date the interpretation of such experiments has relied on a number of untested assumptions. The similarity of the expected profile for the cholera toxin B-subunit pentamer and the measured profile (Krasilnikov et al., 1991) shows that the methodology set out in this work could potentially lead to the ability to reliably link such measurements to structural parameters. It has already been demonstrated that great care needs to be taken in interpreting any "characteristic radius" (or diameter) for a channel. In terms of conductance or permeability, the most important parameter is likely to be the minimum radius of the channel, which is likely to occur around the point where the ratio profile starts to rise (Fig. 8). The mid-effect point will be at a larger radius, and the turning point as interpreted by Krasilnikov et al. (1991, 1992) is likely to be close to the end radius (Fig. 8).

In two studies to date (Bezrukov and Vodyanoy, 1993; Korchev et al., 1995), the fact that similar ratio profiles have been found for different conductance states of a channel has led to important assertions. For alamethicin channels Bezrukov and Vodyanoy (1993) interpreted the similar conductance ratio profile for the three states studied as contradicting the widely accepted barrel stave hypothesis (Fox and Richards, 1982; Sansom, 1993). In relation to this, it is instructive to compare the results of that study with those obtained for the cholera toxin B-subunit pentamer (Krasilnikov et al., 1991).

As shown in Fig. 10, the normalized profiles are practically coincident for the cholera toxin B-subunit pentamer and all three alamethicin conductance states, with the exception of the value at large molecular weight/hydrodynamic radius. The fact that cholera toxin B-subunit pentamer and alamethicin conductance state 2 (identified here with a seven-helix bundle) have similar molar conductances can be added to this. However, alamethicin is very unlikely to be able to adopt a structure that is similar to cholera toxin B-subunit pentamer. The crystal structure of alamethicin (Fox and Richards, 1982) reveals that the helix is bent. This is in contrast to the straight helices that line the central pore of cholera toxin B-subunit pentamer. From this the conclusion can be drawn that dissimilar structures can result in similar conductance profiles. As a consequence, it may be that the data for alamethicin are in fact compatible with the barrel stave hypothesis. More credence can be added to this interpretation by the values found for the end radius for the various states from access resistance considerations (Table 6). These seem to be compatible with the barrel stave hypothesis.

TABLE 6 Comparing the effective end radii of alamethicin conductance states

Conductance state	Experimental end radius (Å)	Ensemble mean effective end radius (Å)	MD mean effective end radius (Å)
$N = 6, C = 1$	5.2–7.0	5.9	6.2
$N = 7, C = 2$	9.6–11.1	7.1	7.3
$N = 8, C = 3$	10.9–12.4	7.7	8.2

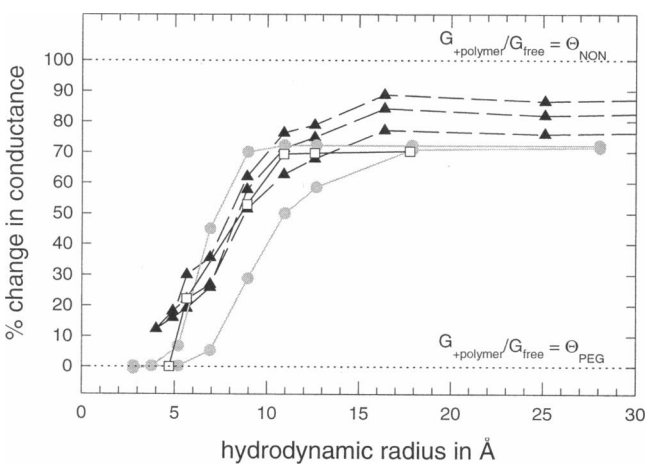

FIGURE 10 A comparison between experimental results found for different ion channels using the polymer exclusion method. The dashed lines with data points marked by triangles are the results found by Bezrukov and Vodyanoy (1993) for three different conductance states of the alamethicin channel. The open squares and solid line mark the result found for cholera toxin B-pentamer by Krasilnikov et al. (1991). The gray circles and lines show results for two different conductance states of *Staphylococcus aureus* α-toxin (Korchev et al., 1995). All data were measured from the relevant publication using a STOE ratchet film measuring device. Molecular weights were converted to hydrodynamic radii by using data from Kuga (1991). As different percentages of nonelectrolyte were used, the data were normalized according to the values of Θ_{PEG} and Θ_{NON} given by Bezrukov and Vodyanoy (1993).

It is also interesting to compare the close grouping of the alamethicin conductance profile and cholera toxin B-subunit pentamer with the result found for *S. aureus* α-toxin by Korchev et al. (1995) (see Fig. 10). Results were obtained for two conductance states of this channel. As the "half effect" radius was similar, the conclusion was drawn that the difference in conductance between the two states could not be accounted for by a simple difference in the size of the internal cavity of the two states. From Fig. 10 it can be seen that the difference between the two conductance states for *S. aureus* α-toxin is much larger than the differences between the three alamethicin states. If the barrel hypothesis is accepted for alamethicin, this would seem to indicate that the *S. aureus* α-toxin data is not necessarily incompatible with a simple steric difference between the two states.

It seems that the parameter most sensitive to differences in structure is the asymptotic value of the conductance ratio. This can be directly linked to the effective end radius for the channel (Bezrukov and Vodyanoy, 1993). It remains to be seen whether such values can be directly correlated to those obtained directly from a high-resolution structure.

These considerations must remain guarded, because at present there is too little concrete information on how the conductance ratio profile relates to the pore dimensions of ion channels when the structure is accurately known. Further detailed experiments are clearly required to obtain consistent profiles for the porins, gramicidin, and cholera toxin B-subunit pentamer. The data obtained could then be critically compared with the results expected, based on the experimental structures available for these channels. It is quite likely that the crude model set out in section 3.2 will need improvement. The result of the study may provide the basis for a simple but reliable way to obtain structural parameters by conductance measurements. Such information could be of crucial importance in guiding modeling studies.

4. CONCLUSIONS

This work shows the importance of systematically linking the conductance properties of a wide variety of ion channels to their three-dimensional structures. Such an approach can provide important guides for the modeling of channels and lead to a better understanding of their behavior. Further progress is now dependent on the detailed examination of the conductance properties of channels of known structure. An important aim of this work is to provide useful tools to scientists working on ion channels. For this reason the program suite HOLE2, which includes facilities to perform all of the calculations set out here, is freely available to all nonprofit organizations (for details see Smart, 1996).

We would like to thank Drs. M. Montal and Mark A. Williams for their constructive advice.

Support by the Wellcome Trust by the provision of a Career Development Fellowship (042889) for OSS and research funding for MSPS is gratefully acknowledged. JB thanks the UK Medical Research Council for providing a research studentship.

REFERENCES

Abola, E. E., F. C. Bernstein, S. H. Bryant, T. F. Koetzle, and J. Weng. 1987. Protein data bank. *In* Crystallographic Databases—Information Content, Software Systems, Scientific Applications. F. H. Allen, G. Bergerhoff, and R. Sievers, editors. Data Commission of the International Union of Crystallography, Bonn, Cambridge, and Chester. 107–132.

Adams, P. D., I. T. Arkin, D. M. Engelman, and A. T. Brünger. 1995. Computational searching and mutagenesis suggest a structure for the pentameric transmembrane domain of phospholamban. *Nature Struct. Biol.* 2:154–162.

Andersen, O. S. 1984. Gramicidin channels. *Annu. Rev. Physiol.* 46: 531–548.

Arseniev, A. S., I. L. Barsukov, V. F. Bystrov, A. L. Lomize, and Yu. A. Ovchinnikov. 1985. ^{1}H-NMR study of gramicidin A transmembrane ion channel: head-to-head right handed single stranded helices. *FEBS Lett.* 186:168–174.

Benz, R., and K. Bauer. 1988. Permeation of hydrophilic molecules through the outer membrane of gram-negative bacteria: review on bacterial porins. *Eur. J. Biochem.* 176:1–19.

Benz, R., A. Schmid, and R. E. W. Hancock. 1985. Ion selectivity of gram-negative bacterial porins. *J. Bacteriol.* 162:722–727.

Benz, R., A. Schmid, T. Nakae, and G. H. vos-Scheperkeuter. 1986. Pore formation of LamB of *Escherichia coli* in lipid bilayer membranes. *J. Bacteriol.* 165:978–986.

Bernstein, F. C., T. F. Koetzle, G. J. B. Williams, E. F. Meyer, Jr., M. D. Brice, J. B. Rodgers, O. Kennard, T. Shimanouchi, and M. Tasumi. 1977. The protein data bank: a computer-based archival file for macromolecular structures. *J. Mol. Biol.* 112:535–542.

Bezrukov, S. M., and I. Vodyanoy. 1993. Probing alamethicin channels with water-soluble polymers: effect on conductance of channel states. *Biophys. J.* 64:16–25.

Bloom, M. 1995. Trans-membrane peptide and protein structures in fluid membranes via NMR. *Biophys. J.* 69:1631–1632.

Breed, J., P. C. Biggin, I. D. Kerr, O. S. Smart, and M. S. P. Sansom. 1997. Alamethicin channels—modelling via restrained molecular dynamics. *Biochim. Biophys. Acta.* (in press).

Breed, J., R. Sankararamakrishnan, I. D. Kerr, and M. S. P. Sansom. 1996. Molecular dynamics simulations of water within models of ion channels. *Biophys. J.* 70:1643–1661

Cowan, S. W., T. Schirmer, G. Rummel, M. Steiert, R. Ghosh, R. A. Pauptit, J. N. Jansonius, and J. P. Rosenbusch. 1992. Crystal structures explain functional properties of two *E. coli* porins. *Nature.* 358:727–733.

Cramer, R. D., D. E. Patterson, and J. D. Bunce. 1988. Comparative molecular field analysis (CoMFA). 1. Effect of shape on binding of steroids to carrier proteins. *J. Am. Chem. Soc.* 110:5959–5967.

Dorman, V., M. B. Partenskii, and P. C. Jordan. 1996. A semi-microscopic Monte Carlo study of permeation energetics in a gramicidin-like channel: the origin of cation selectivity. *Biophys. J.* 70:121–134.

Engels, M., D. Bashford, and M. R. Ghadiri. 1995. Structure and dynamics of self-assembling peptide nanotubes and the channel-mediated water organization and self-diffusion. A molecular dynamics study. *J. Am. Chem. Soc.* 117:9151–9158.

Fettiplace, R., D. M. Andrews, and D. A. Haydon. 1971. The thickness, composition and structure of some lipid bilayers and natural membranes. *J. Membr. Biol.* 5:277–296.

Fox, R. O., and F. M. Richards. 1982. A voltage gated ion channel model inferred from the crystal structure of alamethicin at 1.5 angstrom resolution. *Nature.* 300:325–330.

Ghadiri, M. R., J. R. Granja, and L. K. Buehler. 1994. Artificial transmembrane ion channels from self-assembling peptide nanotubes. *Nature.* 369:301–304.

Ghadiri, M. R., J. R. Granja, R. A. Milligan, D. E. McRee, and N. Khazanovich. 1993. Self-assembling organic nanotubes based on a cyclic peptide architecture. *Nature.* 366:324–327.

Ghadiri, M. R., K. Kobayashi, J. R. Granja, R. K. Chadha, and D. E. McRee. 1995. The structural and thermodynamic basis for the formation of self-assembled peptide nanotubes. *Angew. Chem. Int. Ed. Engl.* 34: 93–95.

Granja, J. R., and M. R. Ghadiri. 1994. Channel-mediated transport of glucose across lipid bilayers. *J. Am. Chem. Soc.* 116:10785–10786.

Hall, J. E. 1975. Access resistance of a small circular pore. *J. Gen. Physiol.* 66:531–532.

Hanke, W., and G. Boheim 1980. The lowest conductance state of the alamethicin pore. *Biochim. Biophys. Acta.* 596:456–462.

Head, R. D., M. L. Symthe, T. I. Oprea, C. L. Waller, S. M. Green, and G. R. Marshall. 1996. VALIDATE: a new method for the receptor-based prediction of binding affinities of novel ligands. *J. Am. Chem. Soc.* 118:3959–3969.

Henderson, R., J. M. Baldwin, T. A. Ceska, F. Zemlin, E. Beckman, and K. H. Downing. 1990. Model for the structure of bacteriorhodopsin based on high-resolution electron cryo-microscopy. *J. Mol. Biol.* 213: 899–929.

Hille, B. 1992. Ionic Channels of Excitable Membranes, 2nd Ed. Sinauer Associates, Sunderland, MA.

Hladky, S. B., and D. A. Haydon. 1972. Ion transfer across lipid membranes in the presence of gramicidin A. I. studies of the unit conductance channel. *Biochim. Biophys. Acta.* 274:294–312.

Jap, B. K., and P. J. Walian. 1990. Biophysics of the structure and function of porins. *Q. Rev. Biophys.* 23:367–403.

Karshikoff, A., V. Spassov, S. W. Cowan, R. Ladenstein, and T. Schirmer. 1994. Electrostatic properties of two porin channels for *Escherichia coli*. *J. Mol. Biol.* 240:372–384.

Kerr, I. D., R. Sankararamakrishnan, O. S. Smart, and M. S. P. Sansom. 1994. Parallel helix bundles and ion channels: molecular modelling via simulated annealing and restrained molecular dynamics. *Biophys. J.* 67:1501–1515.

Ketchem, R. R., W. Hu, and T. A. Cross. 1993. High-resolution conformation of gramicidin-a in a lipid bilayer by solid-state NMR. *Science.* 261:1457–1460.

Klapper, I., R. Hagstrom, R. Fine, K. Sharp, and B. Honig. 1986. Focusing electric field in the active site of Cu-Zn superoxide dismutase: effect of ionic strength and amino-acid modifications. *Proteins Struct. Funct. Genet.* 1:47–59.

Korchev, Y. E., C. L. Bashford, G. M. Alder, J. Kasianowicz, and C. A. Pasternak. 1995. Low conductance states of a single ion channel are not "closed." *J. Membr. Biol.* 147:233–239.

Kovacs, R. J., M. T. Nelson, H. K. B. Simmerman, and L. R. Jones. 1988. Phospholamban forms Ca^{2+}-selective channels in lipid bilayers. *J. Biol. Chem.* 263:18364–18368.

Krasilnikov, O. V., J. N. Muratkhodjaev, S. E. Voronov, and Y. V. Yezepchuk. 1991. The ionic channels formed by cholera toxin in planar bilayer lipid membanes are entirely attributable to its B-subunit. *Biochim. Biophys. Acta.* 1067:166–170.

Krasilnikov, O. V., R. Z. Sabirov, V. I. Ternovsky, P. G. Merzliak, and J. N. Muratkhodjaev. 1992. A simple method for the determination of the pore radius of ion channels in planar lipid bilayer membranes. *FEMS Microbiol. Immunol.* 105:93–100.

Kreusch, A., and G. E. Schulz. 1994. Refined structure of the porin from *Rhodopseudomonas blastica*: comparison with the porin from *Rhodobacter capsulatus*. *J. Mol. Biol.* 243:891–905.

Kuga, S. 1991. Pore size distribution analysis of gel substances by size exclusion chromatography. *J. Chromatogr.* 206:449–461.

Kuyucak, S., and S. H. Chung. 1994. Temperature dependence of conductivity in electrolyte solutions and ionic channels of biological membranes. *Biophys. Chem.* 52:15–24.

Ludlam, C. F. C., I. T. Arkin, X. M. Liu, M. S. Rothman, P. Rath, S. Aimoto, S. O. Smith, D. M. Engelman, and K. J. Rothschild. 1996. Fourier transform infrared spectroscopy and site-directed isotope labeling as a probe of local secondary structure in the transmembrane domain of phospholamban. *Biophys. J.* 70:1728–1736.

Lynden-Bell, R., and J. C. Rasaiah. 1996. Mobility and solvation of ions in channels. *J. Chem. Phys.* 105:9266–9280.

Merritt, E. A., S. Sarfaty, F. Vandenakker, C. Lhoir, J. A. Martial, and W. G. J. Hol. 1994. Crystal-structure of cholera-toxin B-pentamer bound to receptor g(m1) pentasaccharide. *Protein Sci.* 3:166–175.

Perutz, M. 1992. Protein Structure: New Approaches to Disease and Therapy. W. H. Freeman and Co., New York.

Rempp, P. 1957. Contribution a l'étude des solutions de molécules en chaine a squelette oxygéné. II. Viscosités intrinsequés et cofficients de diffusion de translation des polyoxyéthylènegycols. *J. Chim. Phys.* 54: 432–453.

Revah, F., D. Bertrand, J.-L. Galzi, A. Devillers-Thiéry, C. Mulle, N. Hussy, S. Bertrand, M. Ballivet, and J.-P. Changeux 1991. Mutations in the channel domain alter desensitization of a neuronal nicotinic receptor. *Nature.* 353:846–849.

Robinson, R. A., and R. H. Stokes. 1959. Electrolyte Solutions: The Measurement and Interpretation of Conductance, Chemical Potential and Diffusion in Solutions of Simple Electrolytes, 2nd Ed. Butterworths Scientific Publications, London.

Roux, B. 1995. Theory of transport in ion channels: from molecular dynamics simulations to experiments. *In* Computer Modelling in Molecular Biology. J. M. Goodfellow, editor. VCH, Weinham. 133–169.

Roux, B., and M. Karplus. 1991a. Ion transport in a gramicidin-like channel—dynamics and mobility. *J. Phys. Chem.* 95:4856–4868.

Roux, B., and M. Karplus. 1991b. Ion transport in a model gramicidin channel—structure and thermodynamics. *Biophys. J.* 59:961–981.

Roux, B., and M. Karplus. 1993. Ion transport in the gramicidin channel—free-energy of the solvated right-handed dimer in a model membrane. *J. Am. Chem. Soc.* 115:3250–3262.

Sankararamakrishnan, R., C. Adcock, and M. S. P. Sansom. 1996. The pore domain of nicotinic acetylcholine receptor: molecular, modelling, pore dimensions and electrostatics. *Biophys. J.* 71:1659–1671.

Sansom, M. S. P. 1993. Structure and function of channel-forming peptaibols. *Q. Rev. Biophys.* 26:365–421.

Sansom, M. S. P., and I. D. Kerr. 1995. Transbilayer pores formed by β-barrels: molecular modeling of pore structures and properties. *Biophys. J.* 69:1334–1343.

Sansom, M. S. P., R. Sankararamakrishnan, and I. D. Kerr. 1995. Modelling membrane proteins using structural restraints. *Nature. Struct. Biol.* 2:624–631.

Schirmer, T., T. A. Keller, Y.-F. Wang, J. P. Rosenbusch. 1995. Structural basis for sugar translocation through maltoporin channels at 3.1 Å resolution. *Science.* 267:512–514.

Selley, N. J. 1977. Experimental Approach to Electrochemistry. Edward Arnold, London.

Simmerman, H. K. B., D. E. Lovelace, and L. R. Jones. 1989. Secondary structure of detergent solubilized phospholamban, a phophorylatable oligmeric protein of cardiac sarcoplasmic reticulum. *Biochim. Biophys. Acta.* 997:322–329.

Smart, O. S. 1991. Simulation of a conformational rearrangement of the substrate in D-xylose isomerase. DIC/Ph.D. thesis. Imperial College University of London, London.

Smart, O. S. 1994. A new method to calculate reaction paths for conformational transitions of large molecules. *Chem. Phys. Lett.* 222:503–512.

Smart, O. S. 1995. Path energy minimization: a new method for the simulation of conformational transitions. *In* Computer Modelling in Molecular Biology. J. M. Goodfellow, editor. VCH, Weinham. 215–240.

Smart, O. S. 1996. Documentation for the HOLE suite of programs. Available on the world wide web at http://www.cryst.bbk.ac.uk/~ubcg8ab/hole/top.html.

Smart, O. S., and J. M. Goodfellow. 1995. On the simulation of conformational transitions: smoothing path energy minimization results. *Mol. Simul.* 14:291–302.

Smart, O. S., J. M. Goodfellow, and B. A. Wallace. 1993. The pore dimensions of gramicidin A. *Biophys. J.* 65:2455–2460.

Syganow, A., and E. von Kitzing. 1995. Integral weak diffusion and diffusion approximations applied to ion-transport through biological ion channels. *J. Phys. Chem.* 99:12030–12040.

Tosteson, M. T., and D. C. Tosteson. 1978. Bilayers containing gangliosides develop channels when exposed to cholera toxin. *Nature.* 275: 142–144.

Unwin, N. 1993. Nicotinic acetylcholine receptor at 9 Å resolution. *J. Mol. Biol.* 229:1101–1124.

Unwin, N. 1995. Acetylcholine receptor channel imaged in the open state. *Nature.* 373:37–43.

Warwicker, J., and H. C. Watson. 1982. Calculation of the electrostatic potential in the active site cleft due to α-helix dipoles. *J. Mol. Biol.* 157:671–679.

Weiner, S. J., P. A. Kollman, D. A. Case, U. C. Singh, C. Ghio, G. Alagona, S. Profeta, and P. Weiner. 1984. A new force field for the simulation of nucleic acids and proteins. *J. Am. Chem. Soc.* 106: 765–784.

Weiss, M. S., and G. E. Schulz. 1992. Structure of porin refined at 1.8 Å resolution. *J. Mol. Biol.* 227:493–509.

Woolley, G. A., and B. A. Wallace. 1992. Model ion channels—gramicidin and alamethicin. *J. Membr. Biol.* 129:109–136.

You, S., S. Peng, L. Lien, J. Breed, and G. A. Woolley. 1996. Engineering stabilized ion channels: covalent dimers of alamethicin. *Biochemistry.* 35:6225–6232.

Zhang, R. -G., D. L. Scott, M. L. Westbrook, S. Nance, B. D. Spangler, G. G. Shipley, and E. M. Westbrook. 1995. The three-dimensional crystal structure of cholera toxin. *J. Mol. Biol.* 251:563–573.